Proceedings of ASME Turbo Expo 2011
GT2011
June 6-10, 2011, Vancouver, British Columbia, Canada

GT2011-45264

ROTORYDNAMIC FORCE COEFFICIENTS OF BUBBLY MIXTURE ANNULAR PRESSURE SEALS

Luis San Andrés
Mast-Childs Tribology Professor, Fellow ASME

Lsanandres@tamu.edu
Mechanical Engineering Department
Texas A&M University
College Station, Texas 77843-3123, USA

ABSTRACT
As oil fields deplete, in particular in deep sea reservoirs, pump and compression systems work under more strenuous conditions with gas in liquid and liquid in gas mixtures, mostly inhomogeneous. Off-design operation affects system overall efficiency and reliability, including penalties in leakage and rotordynamic performance of secondary flow components, namely seals. The paper details a bulk-flow model for annular damper seals operating with gas in liquid mixtures. The analysis encompasses all-liquid and all-gas seals, as well as seals lubricated with homogenous (bubbly) mixtures, and predicts the static and dynamic force response of mixture lubricated seals; namely: leakage, power loss, reaction forces and rotordynamic force coefficients, etc., as a function of the mixture volume fraction (β_S), supply and discharge pressures, rotor speed, whirl frequency, etc. A seal example with a Nitrogen gas mixed with light oil is analyzed. The large pressure drop (70 bar) causes a large expansion of the gas within the seal even for (very) small gas volume fractions (β_S). Predictions show leakage and power loss decrease as $\beta \rightarrow 1$; albeit at low β_S (<0.3) (re)laminarization of the flow and an apparent increase in mixture viscosity, produce a hump in power loss. Cross-coupled stiffnesses and direct damping coefficients decrease steadily with increases in the gas volume fraction; however some anomalies are apparent when the flow turns laminar. Mixture lubricated seals show frequency dependent force coefficients. The equivalent damping decreases above and below β_S~0.10. The direct stiffness coefficients show atypical behavior: a low β_S=0.1 produces stiffness hardening as the excitation frequency increases. Recall that an all liquid seal has a dynamic stiffness softening as frequency increases due to the apparent fluid mass. The predictions call for an experimental program to quantify the static and dynamic forced performance of annular seals operating with (bubbly) mixtures and to validate the current predictive model results.

INTRODUCTION
Annular (damper) seals restrict secondary leakage between stages in centrifugal pumps and compressors. The working fluid is a process liquid of light viscosity or a process gas. Annular seals, although similar in shape to cylindrical journal bearings, have a distinct flow structure driven by flow turbulence and fluid inertia effects. Operating characteristics unique to seals are the large axial pressure gradients and large clearance to radius ratios, while the axial development of the circumferential swirl velocity is responsible for generating cross-coupled (hydrodynamic) forces [1]. Seal rotordynamic force coefficients are of primary influence on the stability and dynamic forced response of high-performance pumps and compressors [2,3]. Textured stator surfaces (macro roughness) [4] reducing the impact of undesirable cross-coupled dynamic forces and improving system stability are by now common practice in damper seal technology. Further, engineered gas damper seals with honeycombs, round hole patterns, etc, render frequency dependent force coefficients (stiffness and damping) [5] that can be tailored to produce significant (large) damping or centering stiffnesses within particular frequency ranges [6]. This fundamental development permits to make of seals load bearing elements and increasing the rotor-bearing system damping ratio (logarithmic decrement) well above accepted (standard) industrial specifications.

Annular seals operate with either a liquid (pump) or a gas (compressor), seldom with a mixture of both. Childs [2] details separately the bulk-flow analyses of liquid annular seals and gas seals and presents comparisons to experimental results published until 1993. The literature on annular seals operating with gas/liquid mixtures or with actual fluid vaporization (phase change) within the seal is scant. Presently, as oil fields deplete compressors work under more strenuous (off-design) conditions with liquid in gas mixtures, mostly inhomogeneous. Similarly, oil compression station pumps operate with gas in liquid mixtures that affect the pumps overall efficiency and reliability. Little is known about seals operating under these conditions, except that the gaseous content travelling with the main liquid affects the seal leakage, power loss and rotordynamic force coefficients; perhaps even inducing random vibrations that are transmitted to the whole rotor-bearing system.

A test program aiming to identify seal force coefficients operating with mixtures is presently relevant. Recall that these (linearized) force coefficients represent changes in reaction forces to small amplitude motions about an equilibrium position. The typical linear model is

$$\mathbf{F} = -\mathbf{K}\,\mathbf{z} - \mathbf{C}\,\dot{\mathbf{z}} - \mathbf{M}\,\ddot{\mathbf{z}} \tag{1}$$

$$\begin{Bmatrix} F_X \\ F_Y \end{Bmatrix} = -\begin{bmatrix} K_{XX} & K_{XY} \\ K_{YX} & K_{YY} \end{bmatrix}\begin{Bmatrix} x \\ y \end{Bmatrix} - \begin{bmatrix} C_{XX} & C_{XY} \\ C_{YX} & C_{YY} \end{bmatrix}\begin{Bmatrix} \dot{x} \\ \dot{y} \end{Bmatrix} - \begin{bmatrix} M_{XX} & M_{XY} \\ M_{YX} & M_{YY} \end{bmatrix}\begin{Bmatrix} \ddot{x} \\ \ddot{y} \end{Bmatrix}$$

where $\mathbf{F}=\{F_X,\ F_Y\}^{\mathrm{T}}$ and $\mathbf{z}=\{x_{(t)}\ ,y_{(t)}\}^{\mathrm{T}}$ are vectors of lateral reaction forces and displacements, respectively. The matrices **K, C** and **M** contain the stiffness, damping and inertia force coefficients, respectively. Fluid inertia or added coefficients (**M**) are significant in seals with dense fluids operating at high speeds and with large pressure differentials.

In general, liquid seal dynamic force coefficients are frequency independent; and thus, the physical **K**-**C**-**M** model is adequate. However, fluid compressibility (in damper seals) leads to stiffnesses that grow with excitation frequency (ω) while the damping coefficient first raises with frequency to later drop dramatically [5,6]. Hence, $\mathbf{K}=\mathbf{K}_{(\omega)}$ and $\mathbf{C}=\mathbf{C}_{(\omega)}$. Ths formulation includes the simple model $\mathbf{K}_{(\omega)}=\mathbf{K}-\omega^2\mathbf{M}$. Note that in gas damper seals, equivalent stiffness (K_e) and damping (C_e) coefficients are complicated functions of frequency; $\mathbf{M}_{(\omega)}$ does not represent physical added masses **[**5].

Cryogenic liquid seals can undergo phase changes. Beatty and Hughes [7] introduced a unique thermohydrodynamic flow model and delivered predictions for an inter stage seal of the (SSME) High-Pressure Oxidizer Turbo-Pump (HPOTP). Seal leakage is reduced by a clearance reduction, increase in rotor speed, lengthening of the seal, and vapor production. Sub cooling of the liquid before the seal inlet reduces vapor production, thereby increasing the leakage.

Iwatsubo and Nishino [8] conducted a test program to quantify the effects of air in water mixtures, volume fractions up 70%, on the dynamic force coefficients of a low pressure, low speed annular seal. The experiments show the fluid film radial and tangential forces decreasing rapidly as the mixture volume fraction increases. More importantly, however, is a reduction of the whirl frequency ratio (a ratio of destabilizing to stabilizing forces) for mixtures with volume fraction equal to 25%. Note that in spite of the large air in water volume fractions used in the tests, the large difference in densities between the two mixture components gives small mass concentrations of gas in terms of mixture quality. The authors also report the onset of random rotor vibrations at mixture volume fractions higher than 70%. These motions, attributed to fluid compressibility, contributed to the great variability in the experimental results.

Arauz and San Andrés [9] developed a two-phase flow analysis for cryogenic fluid seals operating near the critical point or slightly sub-cooled regions. Depending on the supply conditions, three flow regions are likely to occur: all-liquid, liquid-vapor, and all-vapor. Hence, the flow model implemented is a "continuous" vaporization model, as in Ref. [7]. Predictions for static seal characteristics, namely leakage and axial pressure drop, correlate well with published data for a gaseous nitrogen seal and a liquid nitrogen seal with two-phase occurring at the discharge plane [10]. The most important effect occurs when the transition from liquid to mixture takes place within the seal. The large changes in fluid compressibility as it goes form a liquid to a low quality mixture within a short physical distance induce a significant change in the seal dynamic force coefficients, namely a raise in direct stiffness and a drop in cross-coupled stiffness (and whirl frequency ratio). Iwatsubo and Nishino [8] made a similar finding in a water seal with a mixture of low gaseous mass content.

San Andrés el al. [11-16] conducted an experimental and analytical research program on squeeze film dampers (SFDs) aiming to qualify the differences between lubricant cavitation and air ingestion [13-15] and to quantify these effects on a damper dynamic force response [12,15,16]. Note that lubricant cavitation usually means liquid vaporization at pressures near zero absolute or, most likely, release of dissolved gas content at subambient pressures [17]. On the other hand, air ingestion and entrapment is a complicated phenomenon, pervasive to the operation of open ends SFDs with low levels of external pressurization (small flow rates), as is the case in aircraft engines. In experiments conducted with bubbly mixtures (air in oil) with small to large air volume fractions [15], San Andrés et al. found that the damping force coefficients decrease rapidly as the air volume content increases and when the damper journal executed circular centered motions (small to moderate orbit radii). On the other hand, further experiments with controlled bubbly oil mixtures evidenced that unidirectional loads, single frequency or impact (short duration), produced very different damping coefficients [16]. Periodic loads rendered near constant damping coefficients irrespective of the air volume content, except for a dramatic drop with an air only *lubricated* damper (100% air volume fraction). It appears that even minute (discrete) amounts of oil within the damper film lands are enough to produce significant levels of damping. Impact load tests revealed a more interesting behavior with damping coefficients increasing up to 30%, over their all-oil damping magnitude, for gas in oil volume fractions as large as 50%. The small bubbles in the mixture behave as near rigid bodies (not deforming) during the transient (rapid) journal excursions due to the impact loads, and hence appear to increase the mixture effective viscosity. See Ref. [17] for a summary of the research findings, experimental and analytical, stressing that air ingestion in SFDs is device dependent and noting that bubbly mixtures produce force coefficients that are a function of the load action and path, i.e., dampers have memory!

Overly complicated continuum theories [18] and lack of firm experimental evidence and empirical correlations for stress relationships among components make the modeling of multiple-phase flows complicated. Simplified theories, as in Ref. [12] for example, assume a homogenous mixture with the components traveling at the same speed and with the same stress-strain constitutive models as for a single component. Other models, such as that of Diaz [19] for air ingestion in SFDs, rely on extensive empirical correlations particular to the test element and experimental configuration plus operating conditions.

Presently, the analysis of annular seals operating with gas in liquid mixtures follows the bulk-flow model in Ref. [9]. The model, strictly applicable to a homogenous mixture, reproduces the flow models for liquid seals [20] and gas seals with textured surfaces [21]. The material properties of the components and the gas volume fraction (β) define the mixture density and viscosity. Wall shear stress differences, for simplicity and ignorance mainly, follow the standard formulation for bulk-flow models [22].

ANALYSIS

Figure 1 depicts the geometry of a typical annular seal, nomenclature and coordinate system for analysis. A homogeneous (gas in liquid) mixture flows through the thin annular region between a (textured) stator and a shaft or journal rotating at speed Ω. c denotes the nominal radial clearance for the seal land. The graph shows a textured seal, round-hole pattern type with cell depth H_d. The mixture ingresses into the seal inlet (z=0) at supply pressure (P_S) and temperature (T_S) and exits at $z=L$ at ambient pressure (P_a).

<u>The mixture properties</u> The ideal gas in liquid mixture is homogenous, isothermal, and in thermostatic equilibrium. Both liquid and gas components move as a continuum with the same speed, occupying the same volume[1]. The mixture density (ρ) is [12, 19]

$$\rho = \beta\,\rho_G + (1-\beta)\,\rho_L \tag{2}$$

where ρ_L is the liquid density, ρ_G is the gas density, and β is the gas in liquid volume ratio. Note that $\rho_G << \rho_L$. At the supply condition or seal inlet plane, the gas volume fraction is known and denoted by β_S. The equation of state for the ideal gas is

$$\rho_G = \frac{P}{Z\,\Re_G\,T_S} \tag{3}$$

where $\Re_G$ and Z are the gas constant and compressibility factor, and P denotes the pressure. For a bubbly mixture in equilibrium, the gas volume fraction is solely a function of the mixture pressure [19],

$$\beta = \frac{1}{1+\dfrac{P-P_V-\frac{2}{c}S}{P_{G_S}}\left(\dfrac{1}{\beta_S}-1\right)} \tag{4}$$

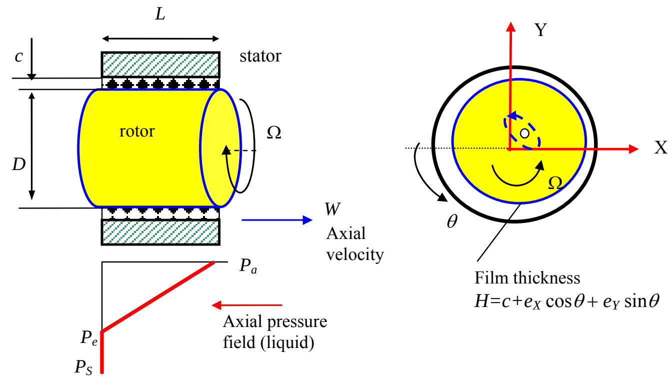

Fig. 1 Geometry of an annular pressure seal and coordinate system

where P_V and S denote the liquid vapor pressure and the surface tension per unit length, respectively. Above, P_{G_S} and β_S are the gas (bubble) pressure and volume fraction at the seal inlet. Note that the term $\left(P_V+\frac{2}{c}S\right)$ is very small, i.e. a few milli-bar, and can be safely disregarded[2]. Ref. [19] explains fully this quasi-static model that ignores bubble dynamics. Incidentally, Refs. [12,14], using a similar model, show predictions correlating well with experimental film pressures and forces recorded with bubbly air in oil mixtures ranging from small to large air volume fractions.

The relationship between the mixture volume fraction (β) and the gas in liquid mass fraction (λ) is

$$\lambda = \frac{\beta\,\rho_G}{\beta\,\rho_G + (1-\beta)\,\rho_L} = \beta\,\frac{\rho_G}{\rho} \tag{5}$$

which is constant throughout the flow domain since there is no phase change, i.e. no liquid vaporization (cavitation)[3].

Formulations for the mixture viscosity differ greatly. Do note that the viscosities of liquids and gases, just like their densities, may differ by two or more orders of magnitude. Most models consider that the viscosity decreases continuously as the mixture quality increases, from its liquid magnitude to that of the gas. However, there is experimental evidence [23,24] showing the mixture viscosity increases[4] above that of the

[1] The flow of two or more material component is rather complex; most mixture flows are neither homogenous nor in thermostatic equilibrium. See Ref. [18] for a scholar work on modeling mixtures as continuum media.

[2] For oil, P_V~0.01 bar and S=0.035 N/m, and with c=0.152 mm, P_V+2S/c=14.6 milli-bar.

[3] Conservation of mass for each component in the mixture is implied. Liquid cavitation is not likely to occur in an annular seal since the pressure supply (P_S) and discharge (P_a) are well above the liquid vapor pressure (P_V).

[4] Chamniprasart [25] states that when the suspension (gaseous phase) is so diluted that the distances between contiguous *particles* are large compared with their dimensions (low gas concentration), the presence of the disperse particles induces an excess of the rate of dissipation of energy over that which occurs if

liquid viscosity magnitude for small mass concentrations of gas in liquid. Presently, the mixture viscosity (McAdams model) is [26]

$$\text{for}\quad \beta \le 0.3 \;\rightarrow\; \frac{\mu}{\mu_L} = 1 + 2.5\left(\frac{\eta+0.4}{\eta+1}\right)\beta \quad ; \quad \eta = \frac{\mu_G}{\mu_L} \qquad (6)$$

$$\text{for}\quad \beta > 0.3 \rightarrow \; \frac{1}{\mu} = \left[\left(\frac{\lambda_+}{\mu_G} - \frac{1}{\mu_+}\right) + \left(\frac{1}{\mu_+} - \frac{1}{\mu_G}\right)\lambda\right]\frac{1}{(\lambda_+ - 1)} \qquad (7)$$

where λ_+ and μ_+, the mixture mass fraction and viscosity at β=0.3; are

$$\lambda_+ = \frac{0.3}{0.3 + 0.7\dfrac{\rho_L}{\rho_G}}; \quad \mu_+ = \frac{1.3\mu_L^2 + 1.75\mu_L\mu_G}{\mu_L + \mu_G} \qquad (8)$$

Note that since $\mu_L >> \mu_G$, then $\mu_+ \sim 1.3\mu_L$ at β=0.3. Other mixture viscosity formulas based on the mass fraction (λ) are not applicable since they would show a constant mixture viscosity within the whole flow domain.

The sound velocity (v_s) for a multiphase mixture with velocity equilibrium between phases is [27]

$$\frac{1}{v_s^2} = \rho\left(\frac{\beta}{\rho_G\, v_{s_G}^2} + \frac{1-\beta}{\rho_L\, v_{s_L}^2}\right) \qquad (9)$$

where the gas and liquid sound speeds are

$$v_{s_G} = \sqrt{\gamma \Re_G T_S} \text{ and } v_{s_L} = \sqrt{\frac{\kappa}{\rho_L}} \qquad (10)$$

with γ is the ratio of specific heats for the gas, and κ is the liquid bulk modulus. Note that the mixture sound speed is a highly sensitive to small changes in the volume fraction; even for β<<1, note that $v_s << v_L$ and v_G.

The bulk-flow equations Within the annular seal P denotes the mixture pressure and $\{U, W\}$ represent the circumferential and axial bulk-flow velocities along the circumferential ($x=R\theta$) and axial directions (z), respectively. The equations for mass conservation and circumferential and axial momentum transport for the homogenous mixture with material properties (ρ, μ) are [9, 20, 21]

$$\frac{\partial}{\partial t}\left(\rho\{H + H_d\}\right) + \frac{\partial}{\partial x}(\rho U H) + \frac{\partial}{\partial z}(\rho W H) = 0 \qquad (11)$$

$$-H\frac{\partial P}{\partial x} + \tau_x\Big]_0^H = \frac{\partial}{\partial t}(\rho U H) + U\frac{\partial}{\partial t}(\rho H_d) + \frac{\partial}{\partial x}\left(\rho U^2 H\right) + \frac{\partial}{\partial z}(\rho U W H) \qquad (12)$$

$$-H\frac{\partial P}{\partial z} + \tau_z\Big]_0^H = \frac{\partial}{\partial t}(\rho W H) + W\frac{\partial}{\partial t}(\rho H_d) + \frac{\partial}{\partial x}(\rho U W H) + \frac{\partial}{\partial z}\left(\rho W^2 H\right) \qquad (13)$$

where $$H = c + e_{X_{(t)}}\cos(\theta) + e_{Y_{(t)}}\sin(\theta) \qquad (14)$$

is the film thickness in the seal land. Above (e_X, e_Y) are the X and Y components of the rotor eccentricity (e). The wall shear stress differences follow the customary functional forms [21]

$$\tau_z\Big]_0^H = -\frac{\mu}{H}(k_z W); \quad \tau_x\Big]_0^H = -\frac{\mu}{H}\left(k_x U - k_r\frac{R\Omega}{2}\right) \qquad (15)$$

Salhi et al. [28] demonstrate the validity of the shear stress model for two-phase mixtures with low gas mass concentrations. The turbulent shear parameters (k_z, k_x, k_r) are local functions of the friction factors (f_r and f_s) relative to the rotor and stator surfaces. Presently, Moody's friction factor formulas (see Nomenclature) are used for simplicity; other empirical relationships are also available [2].

Boundary conditions At the seal inlet plane (z=0), the supply pressure ($P=P_S$) and mixture gas/liquid volume ratio ($\beta=\beta_S$) are specified. At the seal exit plane ($z=L$), the pressure is ambient ($P=P_a$), while the mixture volume fraction is readily determined from Eq. (4).

At z=0, the circumferential velocity $U_{z=0} = \alpha\Omega R$, where α is an entrance or pre-swirl ratio. Fluid inertia causes a sudden pressure drop at the seal inlet; the inlet pressure into the seal is a function of the axial flow velocity [2],

$$P_{z=0} = P_S - \frac{1}{2}\rho(1+\xi)W_{z=0}^2 \qquad (16)$$

where ξ is an empirical entrance loss coefficient[5].

Perturbation analysis To determine the seal force coefficients, consider small amplitude motions $(\Delta e_X, \Delta e_Y) << c$ about the seal static equilibrium position $\left(e_{X_o}, e_{Y_o}\right)$. The motions have whirl frequency (ω). The film thickness and flow variables Φ = (U, W, P) as well as the fluid mixture properties are expressed as

$$H = H_o + (\Delta e_X \cos\theta + \Delta e_Y \sin\theta)e^{i\omega t}; i = \sqrt{-1}$$
$$\Phi = \Phi_o + (\Phi_X \cos\theta + \Phi_Y \sin\theta)e^{i\omega t} \qquad (17)$$

Substitution of Eq. (17) into the bulk-flow equations (11-14) leads to zeroth and first order equations for the equilibrium and perturbed flow fields. These equations are not detailed here for brevity; see Ref. [20] instead.

Solution of the zeroth-order equation gives the seal leakage, reaction forces, drag torque and power losses, as well as the velocities, pressure and mixture composition fields within the seal. The seal mass leakage ($\dot{m}$) and reaction forces $(F_X, F_Y)_o$ follow from

---

the particles were removed and their space is filled with the base fluid; hence the increase in viscosity.

[5] This coefficient denotes a deviation from the inviscid flow condition. ξ must be determined experimentally.

$$\dot{m} = \int_{0}^{2\pi R} \left(\rho H W\right)_{z=L} R\, d\theta \quad (18)$$

$$\begin{Bmatrix} F_{X_o} \\ F_{Y_o} \end{Bmatrix} = -\int_0^L \int_0^{2\pi} P_o \begin{Bmatrix} \cos\theta \\ \sin\theta \end{Bmatrix} R\, d\theta\, dz \quad (19)$$

Solution of the first-order pressure fields allows the evaluation of the seal dynamic force coefficients. Integration of the first order pressure fields on the rotor surface gives a set of four impedance coefficients, $H_{\alpha\beta=X,Y}$,

$$\begin{bmatrix} H_{XX} & H_{XY} \\ H_{YX} & H_{YY} \end{bmatrix} = -\int_0^L \int_0^{2\pi} \begin{bmatrix} P_X \cos\theta & P_Y \cos\theta \\ P_X \sin\theta & P_Y \sin\theta \end{bmatrix} R\, d\theta\, dz \quad (20)$$

The real and imaginary parts of the impedance coefficients render dynamic stiffness and damping coefficients, both frequency dependent, i.e.

$$K_{\alpha\beta_{(\omega)}} + i\,\omega\, C_{\alpha\beta_{(\omega)}} = H_{\alpha\beta_{(\omega)}},\ \alpha,\beta = X, Y \quad (21)$$

Furthermore, for centered operation (e_o=0) recall that $H_{XX}=H_{YY}$ and $H_{XY}=-H_{YX}$. Incidentally, in a seal operating with an incompressible fluid, the damping coefficients ($C_{\alpha\beta}$) are frequency independent, while

$$K_{\alpha\beta_{(\omega)}} = \left(K_{\alpha\beta_*} - \omega^2 M_{\alpha\beta}\right) \quad (22)$$

where $K_{\alpha\beta_*}$ are the static stiffnesses (null frequency) and $M_{\alpha\beta}$ are the added mass coefficients. On the other hand, gas annular seals, in particular textured seals, show frequency dependent stiffness ($K_{\alpha\beta}$) and damping ($C_{\alpha\beta}$) coefficients not well characterized by the *K-C-M* model in Eq. (1). Kleyhans and Childs [5] derive analytical expressions for evaluation of an effective stiffness (K_e) and damping (C_e) in gas damper seals. For centered seal operation (e=0), the effective force coefficients are[6]:

$$\begin{aligned} K_e &= \mathrm{Re}\left(H_{XX}\right) + \mathrm{Ima}\left(H_{XY}\right) = K_{XX_{(\omega)}} + \omega\, C_{XY_{(\omega)}} \\ C_e\, \omega &= \mathrm{Ima}\left(H_{XX}\right) - \mathrm{Re}\left(H_{XY}\right) = \omega\, C_{XX_{(\omega)}} - K_{XY_{(\omega)}} \end{aligned} \quad (23)$$

Hence, seals operating with a gas/liquid mixture will show stiffness and damping coefficients varying in a complicated manner with the excitation (whirl) frequency.

See Ref. [29] for the algebraic discretization of the flow equations (zeroth and first-order) with a control-volume algorithm in staggered grids. A computer program was generated and an engineering graphical user interface developed for ready interface and friendly interaction. Predictions for liquid (only) and gas (only) seals match exactly other predictions obtained with tools unveiled in Refs. [20, 21, 30].

[6] These equivalent force coefficients are strictly applicable to circular centered motions of small amplitude.

PREDICTIONS FOR A SEAL OPERATING WITH A GAS IN OIL MIXTURE

Iwatsubo and Nishino's reference [8] is the only publication showing experimental results for a water lubricated annular seal operating with increasing volumes of gas making a mixture. Alas the paper provides no details on the seal geometry, supply and discharge pressures, the type of gas used and its material properties, etc.

Presently, predictions from the model advanced refer to a smooth surface seal for installation in a test rig in the laboratory. The maximum operating conditions are 15 krpm in rotor speed and a lubrication system delivering up to 25 GPM (~ 95 LPM) and a feed pressure of 71 bar. Nitrogen gas and oil mixtures will be made with a sparger element. Table 1 details the envisioned seal geometry and material properties for both the lubricant (ISO VG 2) and gas. Mixtures of known gas contents can be easily generated with a sparger element. Prior laboratory experiences demonstrate spargers deliver quite homogeneous mixtures, with bubbles sizes depending on the diameter of the (mesh) holes in the inner tube [15]. Note that too large bubbles at the seal inlet will grow in size as the pressure along the seal drops.

Table 1. Example of seal geometry, operating conditions and mixture component properties

Rotor speed,	Ω	1,047 rad/s (10 krpm)	
Diameter, D	116.8 mm	Supply Temperature, T_S	298.3 K (25 C)
Length, L	87.6 mm	Supply pressure, P_S	71 bar
Clearance, c	126.7 μm	Exit pressure, P_a	1 bar
Smooth seal	r_r=0.0005	r_s=0.001	
Entrance pressure loss, ξ	0.25	Inlet pre-swirl ratio, α	0.50
Exit pressure recovery, C_s	0.0		
Physical properties	**mixture**	at P_S, T_S	
ISO VG 2		**Nitrogen (N_2)**	
Viscosity, μ	2.14 c-Poise	Viscosity, μ	0.0182 c-Poise
Density, ρ	784 kg/m^3	Density, ρ	80.2 kg/m^3
Bulk-modulus, κ	20,682 bar	Molecular weight	28
Surface tension, S	0.035 N/m	Compressibility, Z	1.001
Vapor pressure	0.010 bar	$\gamma=C_P/C_V$	1.48
Sound speed, v_s	1,624 m/s	Sound speed, v_s	361 m/s
		Density at P_a, ρ_a	1.1 kg/m^3

Mixture volume fraction β_S varies (0-1.0)

Figure 2 depicts the predicted seal leakage $(\dot{m})$ decreasing monotonically as the inlet gas volume fraction (β_S) increases from an all liquid to an all gas condition. The graph includes magnitudes of the seal inlet and exit volumetric flow rates for the all liquid and all gas conditions. These magnitudes serve to size the pumping requirements in a test facility. Figure 3 shows the exit or discharge gas volume fraction (β_a) and the mixture mass content (λ). Note that even for small inlet β_S, the exit gas volume ratio is rather large, $(\beta_a \rightarrow 1)$, since the pressure drop across the seal is quite high (70 bar) thus producing a large gas volume expansion at the seal discharge plane. The mass fraction for β_S <0.20 is also quite small, albeit increasing rapidly for large inlet gas volume fractions.

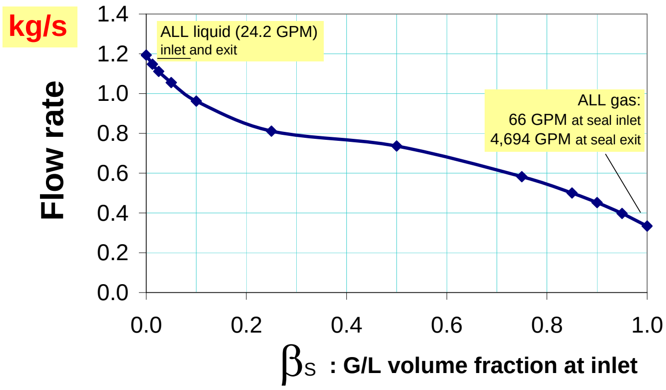

Fig 2. Seal leakage (mass flow rate) versus inlet gas volume fraction (β_S). Mixture N_2 in ISO VG 2 oil (ΔP=71 bar, 10 krpm)

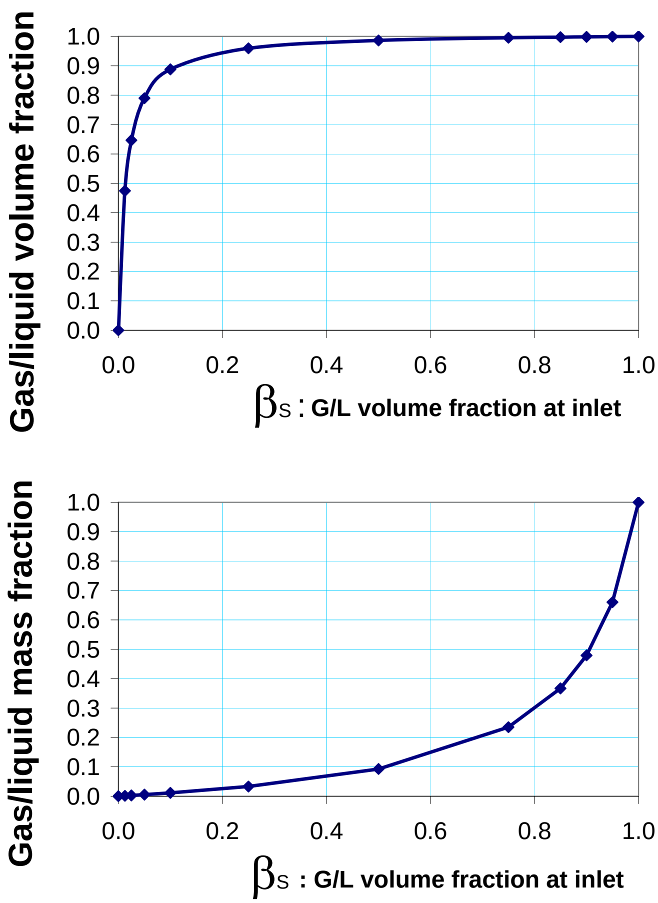

Fig 3. Mixture exit volume fraction (β_a) and mixture mass fraction (λ) versus inlet gas volume fraction (β_S). Mixture N_2 in ISO VG 2 oil (ΔP=71 bar, 10 krpm)

Figure 4 depicts the axial pressure drop across the seal for mixtures with increasing gas content. An all liquid condition, the axial pressure drop is linear; whereas an all gas flow condition shows a nonlinear pressure profile where the pressure drops quickly at the seal exit plane. Most notably, the (inertial) pressure drop at the seal inlet plane is rather small for all mixtures. Viscous effects dominate the flow within the seal since it is rather long (L/D=0.75) with a very tight clearance (c/R=0.002).

Figure 5 shows the (drag) power loss versus the mixture gas volume content. As expected, the gas seal condition generates less power losses since the gas viscosity is a fraction of the liquid viscosity. Note the dip in power loss for β_S~0.1. The sudden decrease and increase may be due to the laminarization of the flow at this mixture condition, as shown by the low mean flow Reynolds numbers (< 2,000) depicted on Figure 6 for small inlet volume fractions (β_S=0.07-0.14). Please see Ref. [31] for a discussion on the transition from turbulent to laminar flow (strictly applicable to a single fluid) and the formulas for friction factors applicable to all flow regimes.

As with most annular pressure seals, the axial flow Reynolds number is much larger than the circumferential flow one. Most importantly, note that for β_S >0.2, the circumferential Reynolds number $\left(\rho_a U_a c \big/ \mu_a \right)$ is rather small since the mixture density is also small. Hence, cross-coupled stiffnesses (K_{XY} =-K_{YX}) expectedly should be small.

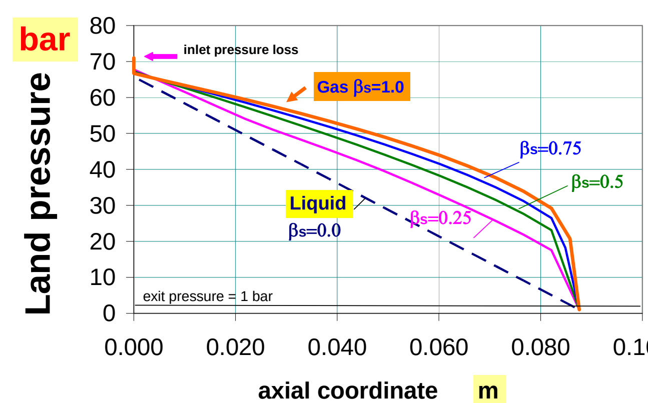

Fig 4. Axial pressure profile in seal for increasing inlet gas volume fractions (β_S). Mixture N_2 in ISO VG 2 oil (ΔP=71 bar, 10 krpm)

Figure 7 depicts the seal dynamic force coefficients (*K*, *C*) evaluated at ω=Ω, i.e., synchronous with rotor speed. Recall that for the centered condition K_{XX}=K_{YY} and K_{XY} =-K_{YX} and C_{XX}=C_{YY} and C_{XY} =-C_{YX}. As expected, both the cross-stiffness (K_{XY}) and direct damping (C_{XX}) decrease as the gas content in the mixture increases, except in the region where the flow becomes laminar at β_S ~0.10. Cross-coupled damping coefficients (C_{XY}) are in general rather small and inconsequential. On the other hand, the direct stiffness (K_{XX}) shows a complicated behavior. Note that for β_S =0.0 (all liquid), the stiffness is negative because of the large added mass of the liquid, i.e., K_{XX}= K_{XXs}- ω^2 M_{XX}.

Figures 8 and 9 show the stiffness and damping force coefficients versus a whirl frequency ratio (ω/Ω) for increasing gas volume fractions (β_S). The graphs demonstrate the frequency dependency of the seal force coefficients, in particular for the direct stiffness K_{XX}. Cross-coupled damping coefficients are a fraction of the direct damping coefficients for nearly all frequency ratios. In general, the cross-stiffness (K_{XY}) and direct damping (C_{XX}) vary little with frequency, both coefficients decreasing quickly as the gas volume content increases. However, note that for β_S ~0.10, both K_{XY} and C_{XX} are larger than for slightly lower and higher volume fractions. The unexpected change is due to the laminar flow condition. Incidentally, recall that for low gas volume ratios (β_S <0.3) the mixture viscosity is higher than that of the liquid, see Eq. (6).

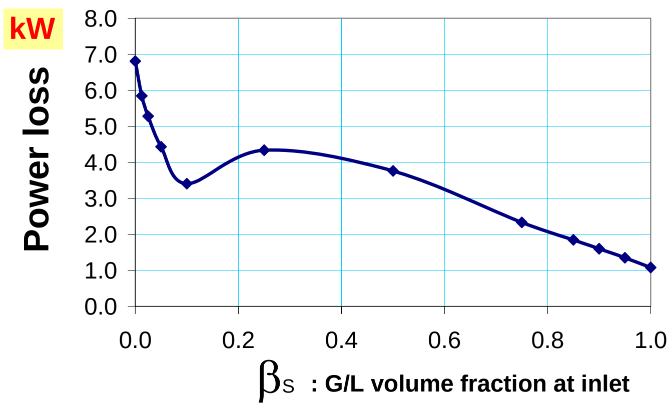

Fig 5. Drag power loss versus inlet gas volume fraction (β_S). Mixture N_2 in ISO VG 2 oil (ΔP=71 bar, 10 krpm)

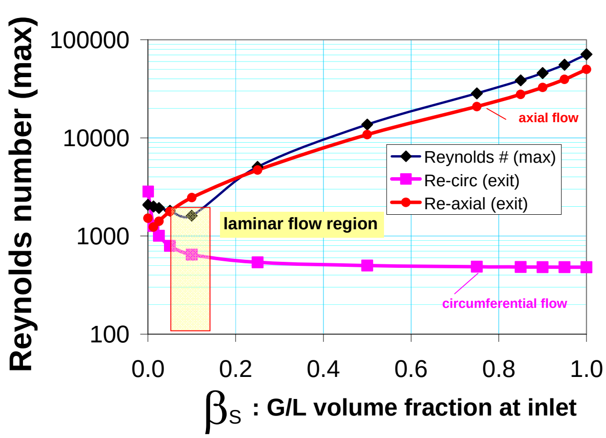

Fig 6. Reynolds numbers: maximum and at exit plane versus inlet gas volume fraction (β_S). Mixture N_2 in ISO VG 2 oil (ΔP=71 bar, 10 krpm)

On the other hand, on Figure 8, note the pronounced variation of the direct stiffness (K_{XX}) with frequency. For the pure liquid condition, β_S=0, the coefficient shows the known dependency $K_{XX}= K_{XXs} -\omega^2 M_{XX}$; M_{XX} ~31 kg. This large added mass is typical for a small clearance, long seal. On the other hand, for large gas volume fractions β_S >0.75, K_{XX} is nearly invariant with frequency. More important however is that for β_S =0.10, the direct stiffness actually increases significantly with frequency. This hardening effect is due to the compressibility of the mixture and the increase in mixture viscosity. Stiffness hardening is typical in textured damper seals, for example, giving negative added mass coefficients.

This prediction is important because, just like in honeycomb and round-hole pattern damper seals, the mixture (bubbles) can be tailored to produce either increased damping or an increased stiffness at particular operating conditions.

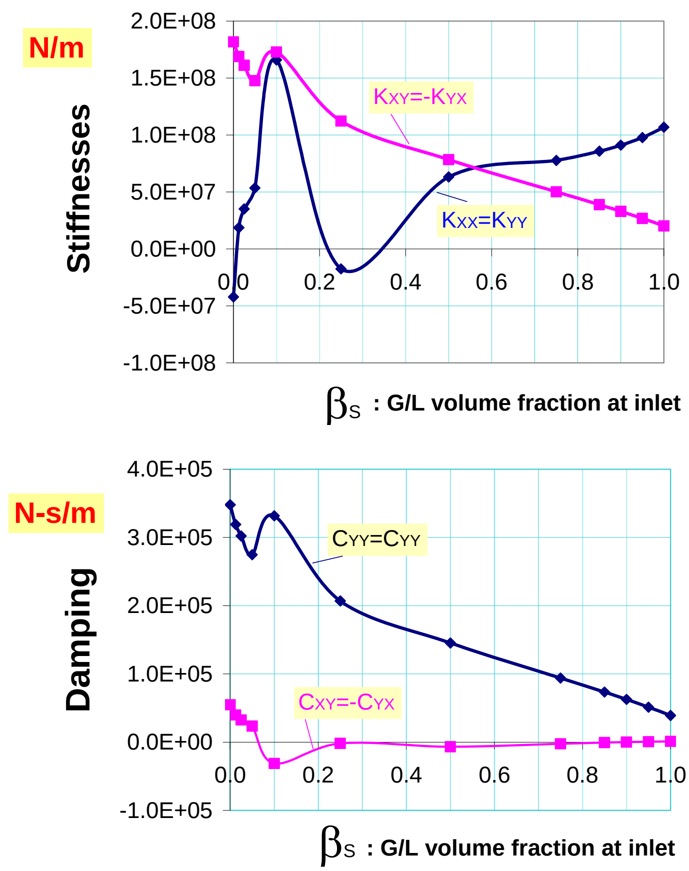

Fig 7. Seal (synchronous) stiffness and damping coefficients versus inlet gas volume fraction (β_S). Mixture N_2 in ISO VG 2 oil (ΔP=71 bar, 10 krpm)

Figure 10 depicts the equivalent stiffness and damping coefficients, strictly applicable to circular centered orbits, $K_e = K_{XX} + \omega C_{XY}$ and $C_e = C_{XX} - \frac{1}{\omega} K_{XY}$, versus the whirl frequency ratio (ω/Ω). Note that C_e=0 at ω/Ω=0.5, as expected for a long seal with an inlet swirl ratio α=0.5. For (ω/Ω)>0.5, the equivalent damping steadily decreases as the inlet gas volume fraction increases above 0.10. On the other hand, the equivalent stiffness K_e shows a more complicated behavior; and just like with K_{XX}, peaks at β_S =0.10 with a strong hardening effect as the whirl frequency (ω) increases.

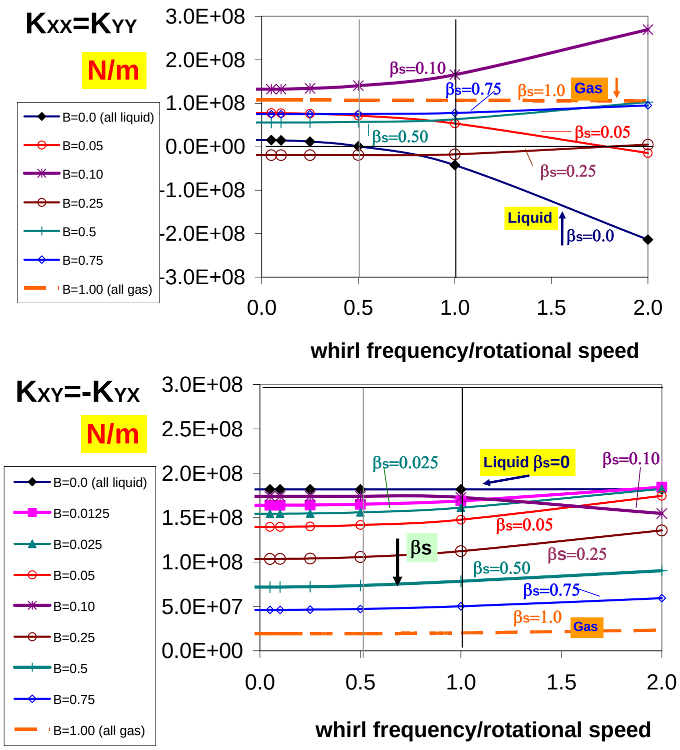

Fig 8. Seal stiffness coefficients versus whirl frequency ratio (ω/Ω) for increasing inlet gas volume fractions (βS). Mixture N_2 in ISO VG 2 oil (Δ*P*=71 bar, 10 krpm)

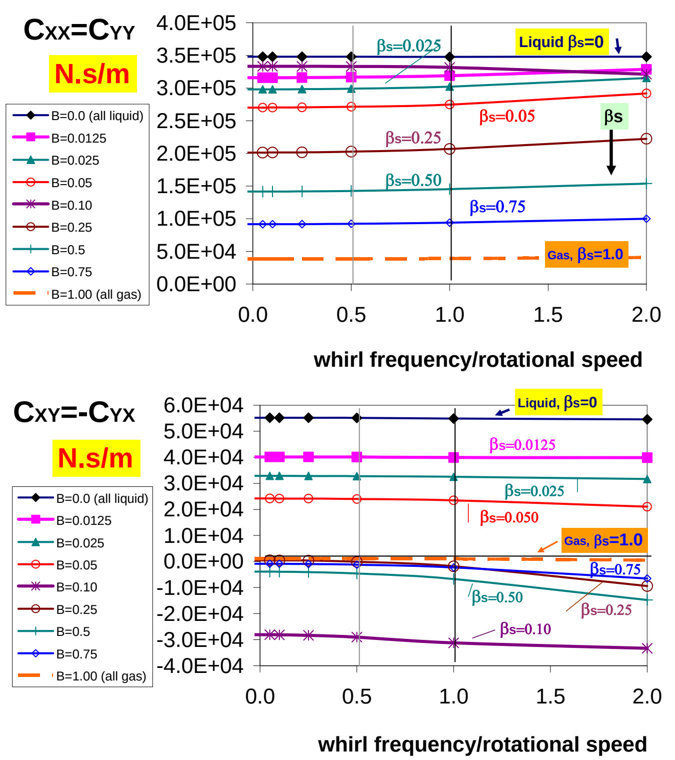

Fig 9 Seal damping coefficients versus whirl frequency ratio (ω/Ω) for increasing inlet gas volume fractions (βS). Mixture N_2 in ISO VG 2 oil (Δ*P*=71 bar, 10 krpm)

CONCLUSIONS

The paper details a bulk-flow analysis for prediction of the flow field and leakage, power loss, reaction forces and dynamic force coefficients for annular damper seals operating with mixtures of gas and liquid. The model assumes a homogenous mixture of two components in thermohydrodynamic equilibrium with identical (bulk-flow) speeds. The analysis also applies to an all liquid seal or an all gas seal.

A mixture, gaseous Nitrogen in light (ISO VG2) oil, and seal geometrical dimensions and operation conditions available in the laboratory (Δ*P*=71 bar, 10 krpm rotor speed*)* were considered for an application example. The pressure drop causes a rather large expansion of the gas along the seal land and at its exit plane.

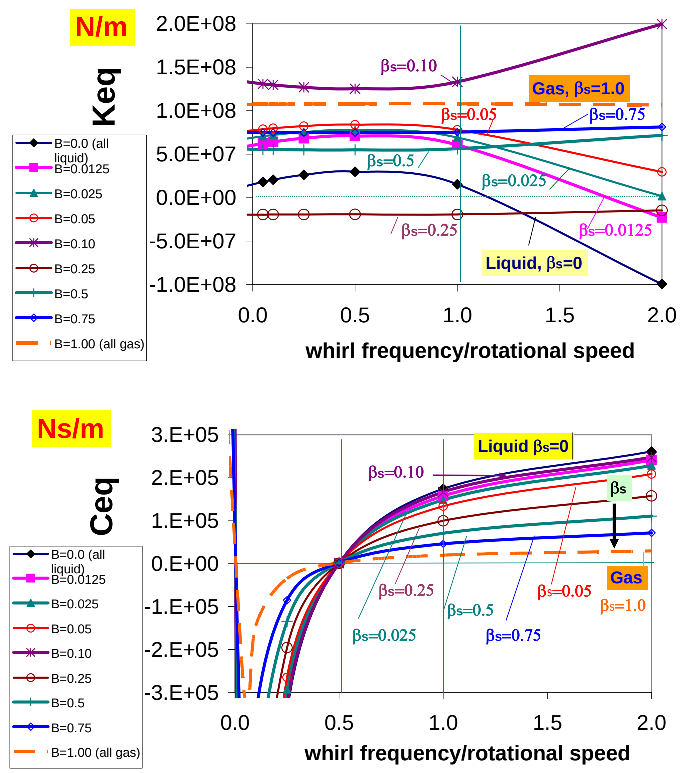

Fig 10. Seal equivalent stiffness (K_e) and damping (C_e) coefficients versus whirl frequency ratio (ω/Ω for increasing inlet gas volume fractions (βS). Mixture N_2 in ISO VG 2 oil (Δ*P*=71 bar, 10 krpm)

The predictions show leakage and power loss steadily decreasing with the gas in liquid volume content, $\beta \rightarrow 1$; albeit at low volume fractions (β_S<0.3) (re)laminarization of the flow and an apparent increase in mixture viscosity, produce a dip in leakage and power loss. Seal rotordynamic force coefficients show strong dependency on the excitation frequency. Cross-coupled stiffnesses and direct damping coefficients decrease steadily with increases in the gas volume fraction; however some anomalies are apparent when the flow is laminar. The direct stiffness coefficients show atypical behavior, in particular a mixture of gas volume fraction β_S=0.1 produces stiffness hardening as the excitation frequency increases. Recall that an (incompressible) all liquid seal has (dynamic) stiffness softening as frequency increases due to the apparent fluid mass.

The extraordinary results justify a comprehensive test program aiming to quantify the static and dynamic forced performance of annular pressure seals operating with (bubbly) mixtures. Resources for the endeavor are presently sought from oil and gas rotating machinery manufacturers and end users.

ACKNOWLEDGEMENTS

The support of the TAMU Turbomachinery Laboratory is gratefully acknowledged. The interest of Professor Dara Childs on seeing this work completed is honored.

NOMENCLATURE

c	Seal radial clearance [m].
C_e	$(C_{XX} - \omega^{-1} K_{XY})$. Equivalent damping [N.s/m]
$C_{\alpha\beta}$	Damping force coefficients [N.s/m], $_{\alpha\beta=X,Y}$
D	Seal diameter [m]
e	Rotor eccentricity [m]
F_X, F_Y	Seal reaction forces, X and Y directions [N].
$f_{r,s}$	Moody's turbulent friction factors at rotor and stator surfaces. $a_m\left[1+\left\{c_m\frac{r_g}{H}+b_m\frac{1}{\mathrm{Re}_{r,s}}\right\}^{1/3}\right]$, a_m=0.001375; b_m=5 x 10^5; c_m=10^4
H	Film thickness [m]
H_d	Effective depth of macro texture in seal surface [m]
$H_{\alpha\beta}$	$(K_{\alpha\beta} + i\omega K_{\alpha\beta})$. Seal impedance [N/m] $_{\alpha\beta=X,Y}$
K_e	$(K_{XX}+\omega\, C_{XX})$. Equivalent stiffness [N/m]
$K_{\alpha\beta}$	Seal stiffness coefficients [N/m], $_{\alpha\beta=X,Y}$
k_r, k_s	$f_s\, Re_s$, $f_r\, Re_r$. Turbulent shear parameters at stator and rotor surfaces
k_x,k_z	$\frac{1}{2}(k_r+k_s)$. Shear stress factors along circumferential and axial directions
L	Seal axial length [m]
$\dot{m}$	Seal mass leakage [kg/s]
$M_{\alpha\beta}$	Mass coefficients [kg] $_{\alpha\beta=X,Y}$
P	Mixture pressure [Pa].
P_S, P_a	Supply and discharge pressures [Pa].
P_V	Liquid vapor pressure [Pa].
P_X, P_Y	First order (perturbed) pressures [Pa/m].
R	$\frac{1}{2}$ D. Journal (shaft) radius [m].
$\Re_G$	Gas constant [J/kg-degK]
Re_r	$\frac{\rho}{\mu}H\left(\left\{U-\frac{1}{2}\Omega R\right\}^2+W^2\right)^{1/2}$. Reynolds number relative to rotor surface
Re_s	$\frac{\rho}{\mu}H\left(U^2+W^2\right)^{1/2}$. Reynolds number relative to stator surface
r_r,r_s	Mean roughness depth at rotor and stator surfaces [m]
S	Liquid surface tension per unit length [N/m].
t	Time [s].
T_S	Supply temperature [degK]
U, W	Bulk-flow velocities (circumferential and axial) [m/s]
v_s	Sound speed [m/s]
X,Y	Inertial coordinate system [m].
$x=R\theta$, z	Circumferential and axial coordinates for flow domain [m].
Z	Gas compressibility factor [-]
α	Entrance swirl factor for circumferential velocity
β	Gas in liquid volume fraction [–]
γ	Gas ratio of specific heats
κ	Liquid bulk-modulus [Pa]
λ	Gas in liquid mass fraction [–]
ξ	Seal inlet pressure loss coefficient [-]
η	μ_G/μ_L. Gas to liquid viscosity ratio [-]
μ	Fluid viscosity [Pa-s]
ρ	Fluid density [kg/m^3]
τ_x, τ_z	Wall shear stress differences, circumferential and axial [Pa]
Ω	Rotor (journal) speed [rad/s]
ω	Rotor whirl frequency [rad/s]

Subscripts

o	Zeroth order solution.
α	perturbations along X, Y
L	Liquid component
G	Gas component
i	Inlet plane conditions
S	Supply condition
+	Mixture properties at β=0.3.

REFERENCES

[1] San Andrés, L., 2010, "Annular Pressure Seals," *Modern Lubrication Theory*, Notes 12a, Texas A&M University Digital Libraries, https://repository.tamu.edu/handle/1969.1/93197

[2] Childs, D., 1993, *Turbomachinery Rotordynamics: Phenomena, Modeling, and Analysis*, John Wiley & Sons, Inc., New York, New York.

[3] Childs, D., and Vance, J., 1997, "Annular Gas Seals and Rotordynamics of Compressors and Turbines", Proc. of the 26th Turbomachinery Symposium, Texas A&M University, Houston, TX, September, pp. 201-220.

[4] von Pragenau, G., 1982, "Damping Seals for Turbomachinery", NASA Technical Paper No. 1987.

[5] Kleynhans, G., and Childs, D., 1997, "The Acoustic Influence of Cell Depth on the Rotordynamic

Characteristics of Smooth-Rotor/Honeycomb-Stator Annular Gas Seals," ASME J. Eng. Gas Turbines Power, **119**, pp. 949-957.
[6] Sprowl, T., and Childs, D., 2007, "A Study of the Effects of Inlet Preswirl on the Dynamic Coefficients of a Straight-Bore Honeycomb Gas Damper Seal," ASME J. Eng. Gas Turbines Power, **129**, pp. 220-229.
[7] Beatty, P.A., and Hughes, W.F., 1987, "Turbulent Two-Phase Flow in Annular Seals," ASLE Trans., **30**, pp. 11-18.
[8] Iwatsubo, T., and Nishino, T., 1993, "An Experimental Study on the Static and Dynamic Characteristics of Pump Annular Seals," *7th Workshop on Rotordynamic Instability Problems in High Performance Turbomachinery*, Texas A&M University, College Station, Texas, May 10-12.
[9] Arauz, G., and San Andrés, L., 1998, "Analysis of Two Phase Flow in Cryogenic Damper Seals, I: Theoretical Model, II: Model Validation and Predictions," ASME J. Tribol., **120**, pp. 221-227, 228-233
[10] Hendricks, R.C., 1987, "Straight Cylindrical Seals for High Performance Turbomachinery," NASA TP-1850.
[11] Tao, L., S. Diaz, L. San Andrés, and K.R. Rajagopal, 2000, "Analysis of Squeeze Film Dampers Operating with Bubbly Lubricants" ASME J. Tribol., 122, pp. 205-210.
[12] Tao, L., Diaz, S., San Andrés, L., and Rajagopal, K.R., 2000, "Analysis of Squeeze Film Dampers Operating with Bubbly Lubricants" ASME J. Tribol., **122**, pp. 205-210
[13] Diaz, S., and San Andrés, L., 2001, "Air Entrainment versus Lubricant Vaporization in Squeeze Film Dampers: An Experimental Assessment of their Fundamental Differences," ASME J. Eng. Gas Turbines Power, **123**, pp. 871-877
[14] Diaz, S., and San Andrés, L., 2001, "A Model for Squeeze Film Dampers Operating with Air Entrainment and Validation with Experiments," ASME J. Tribol., **123,** pp. 125-133.
[15] Diaz, S., and San Andrés, L., 2002, "Pressure Measurements and Flow Visualization in a Squeeze Film Damper Operating with a Bubbly Mixture," ASME J. Tribol., **124**, pp. 346-350.
[16] San Andrés, L., Diaz, S., and Rodriguez, L., 2001, "Sine Sweep Load versus Impact Excitations and their Influence on the Damping Coefficients of a Bubbly Oil Squeeze Film Damper," Tribol. Trans., **44,** pp. 692-698.
[17] San Andrés, L., 2010, "Squeeze Film Dampers: Operation, Models and Technical Issues," *Modern Lubrication Theory,* Notes 14, Texas A&M University Digital Libraries, https://repository.tamu.edu/handle/1969.1/93197
[18] Rajagopal, K. R., and Tao, L., 1995, *Mechanics of Mixtures,* Series on Advance sin Mathematics for Applied Sciences, Vol. 35, World Scientific, Singapore.
[19] Diaz, S., 1999, "The Effects of Air Entrainment on the Forced Performance of Squeeze Film Dampers: Experiments and Analysis," Ph.D. dissertation, Department of Mechanical Engineering, Texas A&M University, May.
[20] San Andrés, L., 1991, "Analysis of Variable Fluid Properties, Turbulent Annular Seals," ASME J. Tribol., **113**, pp. 694-702.
[21] San Andrés, L., and Soulas, T., 2007, "A Bulk Flow Model for Off-Centered Honeycomb Gas Seals," ASME J. Eng. Gas Turbines Power, **129**, pp. 185-194.
[22] San Andrés, L., "Turbulence in Thin Film Flows, *Modern Lubrication Theory,* Notes 8, Texas A&M University Digital Libraries, https://repository.tamu.edu/handle/1969.1/93197
[23] Hayward, A., 1961, "Viscosity of Bubbly Oil," *Fluids Report,* No 99, National Engineering Laboratory.
[24] Zeidan, F.Y., Vance, J.M., 1990, "A Density Correlation for a Two Phase Lubricant and its Effect on the Pressure Distribution," *ASLE Trans.*, **33**, pp. 641-647.
[25] Chamniprasart, K., 1992, "A Theoretical Model of Hydrodynamic Lubrication with Bubbly Oil," Ph.D. Dissertation, Department of Mechanical Engineering, University of Pittsburgh.
[26] McAdams, W.H., Woods, W.K., and Heroman, L.C., Jr., 1942, "Vaporization inside Horizontal Tubes- II -Benzene-Oil Mixtures," ASME Trans., **64**, p.193.
[27] Andrews, M.J., and O'Rourke, P.J., 1996, "The Multiphase Particle-in-Cell (MP-PIC) Method for Dense Particulate Flows," Int. Journal on Multiphase Flow, **22**, pp. 379-402.
[28] Salhi, A., Rey, C., and Rosant, J.M., 1992, "Pressure Drop in Single-Phase and Two-Phase Couette-Poiseuille Flow," ASME J. Fluids Eng., **114,** pp.80-84.
[29] San Andrés, L., 2010, "Thermohydrodynamic Bulk-Flow Model in Thin Film Lubrication," *Modern Lubrication Theory,* Lecture Notes 10, Texas A&M University Digital Libraries, https://repository.tamu.edu/handle/1969.1/93197
[30] XLTRC^2 Rotordynamics Software Suite v 2.1, 2009, Turbomachinery Laboratory, Texas A&M University, College Station, TX.
[31] Zirkelback, N., and L. San Andrés, 1996, "Bulk-Flow Model for the Transition to Turbulence Regime in Annular Seals," Tribol. Trans., **39**, 4, pp. 835-842.